Few-body structures in the mirror nuclei ^{11}O and ^{11}Li

E. Garrido[1] and A. S. Jensen[2]
[1]*Instituto de Estructura de la Materia, IEM-CSIC, Serrano 123, E-28006 Madrid, Spain*
[2]*Department of Physics and Astronomy, Aarhus University, DK-8000 Aarhus C, Denmark*

(Received 3 December 2019; accepted 9 March 2020; published 23 March 2020)

We investigate the dripline mirror nuclei ^{11}Li and ^{11}O, located on the neutron and proton dripline, respectively. We calculate the lowest four states, $3/2^-$, $1/2^+$, $3/2^+$, and $5/2^+$, built on double occupancy in the nuclear $s_{1/2}$ and $p_{1/2}$ valence single-particle states. We use the hyperspherical adiabatic expansion method to solve the three-body problem for a frozen nuclear core surrounded by two identical nucleons. The four analog states in ^{11}O are obtained with precisely the same interactions as used for the four states in ^{11}Li, except for addition of the Coulomb interaction from the charge of the substituted valence protons. Surprisingly, the four energies deviate from each other only by less than a few hundred keV. Any of them could then turn out to be the ground state, due to the uncertainty related to the angular momentum and parity dependence of the three-body potential. Still, our calculations marginally favor the $1/2^+$ state. The structures of these four states in ^{11}O deviate substantially from the analog states in the mirror, ^{11}Li.

DOI: 10.1103/PhysRevC.101.034003

I. INTRODUCTION

Nuclear structure varies tremendously from the many-body leptodermous features of heavy nuclei to the individual properties of light nuclei [1–6]. The unexpected observed increased jump in radius from lighter Li isotopes to ^{11}Li [7,8] triggered the research on halo structures [9] in a number of subfields of physics [10]. Few-body structure was especially efficient to describe the gross features of halos, simply because the degrees of freedom essentially decouple into two groups, where only a few nucleons determine the low-energy properties [10].

The overall properties of ^{11}Li are established as a three-body system with constituents of two neutrons and ^{9}Li [11]. In this connection the spin-spin splitting of the $s_{1/2}$ and $p_{1/2}$ single-neutron states coupled to the $3/2^-$ ground state of ^{9}Li is crucial for the halo properties [12,13]. These halo structures are consistent with reaction information [14–16] even after the binding energy has been measured with better accuracy [17]. The space spanned by these single-particle states provides the $3/2^-$ ground state as well as the dipole-excited states of $1/2^+$, $3/2^+$, and $5/2^+$ [18].

The present investigation is triggered by the recent experiments [19] on the mirror nucleus, ^{11}O, which was preceded by related experiments on ^{10}N [20,21], and quickly followed up by theoretical papers on these and a few neighboring nuclei [22–24]. Several previous publications on ^{11}O and ^{10}N are available [25–27]. The comparison of isobaric analog structures is a classical nuclear discipline, which has provided strong support for the generalization of the isospin concept from nucleons to nuclei [1–3]. Since halo structures only occur near threshold for s and p valence nucleons, as in ^{11}Li, the structure may be strongly influenced even for small energy changes. Thus, mirror nuclei on the driplines are most likely to exhibit larger differences than stable nuclear mirrors [10].

The mirror pair ^{11}Li and ^{11}O are located on the neutron dripline and slightly outside the proton dripline, respectively. Still, both are accessible by experiments, which for ^{11}O largely is possible due to the Coulomb barrier. The major effect is from the Coulomb interaction of the additional protons, which has both direct and indirect influence. The same structure in both nuclei produces an energy difference from the additional charge. However, the structure itself is modified by this extra Coulomb interaction and in turn results in a modified energy.

The total effect of the additional Coulomb interaction is quantified in the Thomas-Ehrman (TE) shift [28,29], which is defined as the energy difference (apart from the neutron-proton mass difference) between analog states in mirror nuclei. This energy shift may depend on the state and probably therefore is especially sensitive to variation of halo structure between analog states in ^{11}Li and ^{11}O [30–32]. The possible structure variation between these analog states may lead to sizable state-dependent Thomas-Ehrman shifts. This may even change the sequence of ground and excited states built on these valence configurations.

The recent experimental activity on ^{11}O and ^{10}N is an opportunity to compare properties in mirrors each located around different nucleon driplines. This has earlier proved to be informative. Previous theoretical investigations already provided a number of details on these nuclei. However, they are a little random as essentially all are incomplete in descriptions of the low-lying states supported by the valence nucleon $s_{1/2}$ and $p_{1/2}$ single-particle states, since only the $3/2^-$ state is considered. The only exception is Ref. [22], where the positive-parity state $5/2^+$ is also investigated.

In general, the connection between these mirror nuclei is not particularly well explored. Furthermore, the previous results are for some reason quantitatively deviating, either due to different methods, interactions, or perhaps accuracy

of some kind. We therefore decided to investigate these low-lying nuclear states by use of our well-established few-body method, which due to the phenomenological input also is both simple and accurate. Thus, in the present paper we report on detailed studies of low-energy properties of ^{11}O in comparison to similar investigations of ^{11}Li. Our purpose is twofold: first, to discuss few-body properties of the specific ^{11}O nucleus and, second, to look for general conclusions by studying this mirror of the prototype of a halo nucleus. Larger differences can be expected for such dripline structures in comparison and in contrast to stable mirror nuclei.

Section II first briefly presents the applied hyperspherical adiabatic expansion method [33], the degrees of freedom, and the choice of interaction form. Section III describes the choice of parameters and the derived properties of the subsystems, ^{10}Li and ^{10}N. Sections IV, V, and VI are devoted to the computed three-body properties of ^{11}O specifically in comparison to ^{11}Li. In Sec. VII we present a summary and the conclusions.

II. SKETCH OF THE METHOD

The three-body calculations will be performed using the well-established hyperspherical adiabatic expansion method described in detail in Ref. [33]. In this method the three-body wave function, with total angular momentum J and projection M, is written as:

$$\Psi^{JM} = \frac{1}{\rho^{5/2}} \sum_n f_n^J(\rho) \Phi_n^{JM}(\rho, \Omega), \tag{1}$$

where ρ is the hyperradius, Ω collects the five hyperangles as defined for instance in Ref. [33], and $f_n^J(\rho)$ are the radial expansion functions. The basis set $\{\Phi_n^{JM}(\rho, \Omega)\}$ used in the expansion above is formed by the eigenfunctions of the angular part of the Schrödinger (or Faddeev) equations,

$$\left[\hat{\Lambda}^2 + \frac{2m\rho^2}{\hbar^2}(V_{12} + V_{13} + V_{23})\right]\Phi_n^{JM} = \lambda_n(\rho)\Phi_n^{JM}(\rho, \Omega), \tag{2}$$

where $\hat{\Lambda}$ is the grand-angular momentum operator [33], V_{ij} is the interaction between particles i and j, m is the normalization mass used to define the Jacobi coordinates [33], and $\lambda_n(\rho)$ is the eigenvalue associated to the angular eigenfunction $\Phi_n^{JM}(\rho, \Omega)$.

In practice, Eq. (2) is solved after the expansion

$$\Phi_n^{JM}(\rho, \Omega) = \sum_q C_q^{(n)}(\rho)\left[\mathcal{Y}^{KL}_{\ell_x \ell_y}(\Omega) \otimes \chi^S_{s_x s_y}\right]^{JM}, \tag{3}$$

where q collects all the quantum numbers $\{K, \ell_x, \ell_y, L, s_x, S\}$, where ℓ_x and ℓ_y are the relative orbital angular momenta between two of the particles and between the third particle and the center of mass of the first two, respectively. The total orbital angular momentum L results from the coupling of ℓ_x and ℓ_y. The quantum number K is the so-called hypermomentum, which is defined as $K = 2\nu + \ell_x + \ell_y$, with $\nu = 0, 1, 2, \ldots$. The dependence on these quantum numbers, ℓ_x, ℓ_y, L, and K, is contained in the usual hyperspherical harmonics, $\mathcal{Y}^{KL}_{\ell_x \ell_y}(\Omega)$, whose definition can also be found in Ref. [33], and which satisfy $\hat{\Lambda}^2 \mathcal{Y}^{KL}_{\ell_x \ell_y} = K(K+4)\mathcal{Y}^{KL}_{\ell_x \ell_y}$. In the same way, s_x is the total spin of two of the particles, which couples to the spin of the third particle, s_y, to give the total spin S. The total spin function is represented in Eq. (3) by $\chi^S_{s_x s_y}$. Finally, L and S couple to the total three-body angular momentum J with projection M.

Obviously, the definition of the $\boldsymbol{x}$ and $\boldsymbol{y}$ coordinates (the Jacobi coordinates) is not unique, since for three-body systems three different sets of Jacobi coordinates can be formed [33]. When solving the Schrödinger equation a choice has to be made, which means that only one of the internal two-body subsystems is treated in its natural coordinate. In this work, however, we solve instead the Faddeev equations, which have the nice property of treating all the three possible sets of Jacobi coordinates on the same footing [33].

The radial functions, $f_n^J(\rho)$, in Eq. (1) are obtained after solving the set of coupled equations

$$\left[-\frac{\partial^2}{\partial\rho^2} + \frac{\lambda_n(\rho) + \frac{15}{4}}{\rho^2} - \frac{2mE}{\hbar^2}\right] f_n^J(\rho) = \sum_{n'} \left[2P_{nn'}(\rho)\frac{\partial}{\partial\rho} + Q_{nn'}(\rho)\right] f_{n'}^J(\rho), \tag{4}$$

where E is the three-body energy and $\lambda_n(\rho)$ is obtained from the angular equation (2). The explicit form and properties of the coupling functions $P_{nn'}(\rho)$ and $Q_{nn'}(\rho)$ can be found in Ref. [33].

The set of equations (4) has to be solved imposing to the radial wave functions the appropriate asymptotic behavior. This is particularly simple for bound states, due to the asymptotic exponential fall-off of the radial wave functions. In order to exploit the simplicity of this asymptotic behavior, we compute resonances (understood as poles of the S matrix) by means of the complex scaling method [34,35]. In this method the three-body energy is allowed to be complex, and the radial coordinates are rotated into the complex plane by an arbitrary angle θ ($\rho \to \rho e^{i\theta}$). Under this transformation, and provided that θ is sufficiently large, the resonance wave function behaves asymptotically as a bound state, i.e., it decays exponentially at large distances, and its complex energy, $E = E_R - i\Gamma_R/2$, gives the resonance energy, E_R, and the resonance width, Γ_R.

Being more specific, after the complex scaling transformation, Eqs. (4) are solved by imposing a box boundary condition. The continuum spectrum is then discretized, and the corresponding discrete energies appear in the complex energy plane rotated by an angle equal to 2θ [34,35]. The resonances show up as discrete points, independent of the complex scaling angle, and they are located out of the cut corresponding to continuum states.

Note that an accurate-enough solution of the three-body problem requires convergence at two different levels. First, one needs convergence in the expansion of the angular eigenfunctions in Eq. (3), which is necessary in order to obtain sufficient accuracy in the λ_n eigenvalues in the radial equations (4). A correct convergence requires inclusion of the relevant $\{\ell_x, \ell_y, L, s_x, S\}$ components, and, for each of them, a sufficiently large value, $K_{\max}$, of the hypermomentum K is also needed. Second, one has to reach convergence as well

TABLE I. The strength parameters, $S_i^{(\ell)}$, in MeV for the Gaussian core-nucleon potentials, $V_i^{(\ell)} = S_i^{(\ell)} e^{-r^2/b^2}$, defined in Eq. (5), with the s and p partial waves as in Ref. [23] (also denoted as P1I in Ref. [16]). We choose the same numerical value, $b = 2.55$ fm, for the range parameter, b, in all terms and partial waves.

ℓ	$S_c^{(\ell)}$	$S_{ss}^{(\ell)}$	$S_{\rm so}^{(\ell)}$
0	−5.4	−4.5	–
1	260.75	1.0	300
2	260	−9.0	−300

in the expansion in Eq. (1), which implies a sufficiently large number of adiabatic terms.

Typically, the convergence in the expansion (1) is rather fast, and for bound states and resonances (after the complex scaling transformation) four or five terms are usually enough. However, the expansion (3) is more demanding, especially when dealing with particles with nonzero spin, since the number of components can increase significantly in accordance with a given total three-body angular momentum J. Also, for extended systems, for which the λ_n functions have to be accurately computed at large distances, the required maximum value of the hypermomentum, $K_{\rm max}$, can be rather large.

Given a three-body system, the key quantities determining its properties are the two-body potentials entering in Eq. (2). In this work we shall assume that the nucleon-nucleon interaction is the Gogny-Pires-Tourreil (GPT) potential described in Ref. [36].

For the core-nucleon potential we choose an interaction, adjusted independently for the different partial waves, each term of the form:

$$V_{Nc}^{(\ell)}(r) = V_c^{(\ell)}(r) + V_{ss}^{(\ell)}(r) \boldsymbol{s}_c \cdot (\boldsymbol{\ell} + \boldsymbol{s}_N) + V_{\rm so}^{(\ell)} \boldsymbol{\ell} \cdot \boldsymbol{s}_N, \quad (5)$$

where $\boldsymbol{\ell}$ is the relative orbital angular momentum between the core and the nucleon, whose intrinsic spins are denoted by $\boldsymbol{s}_c$ and $\boldsymbol{s}_N$, respectively. As shown in Ref. [37], this spin-operator structure, which is consistent with the mean-field description of the nucleons in the core, is crucial for a correct implementation of the Pauli principle.

Obviously, when the interaction involves two charged particles, the Coulomb potential should be added to the interactions described above. In this work we shall describe the core as a uniformly charged sphere with radius equal to the charge radius, which for ^{9}C will be taken equal to 2.5 fm. We assume all nucleons are pointlike particles.

III. THE CORE-NUCLEON SYSTEM

For the case of ^{11}Li (^{9}Li $+n+n$) and its mirror partner, ^{11}O (^{9}C $+p+p$), it is clear that the essential ingredient is the nuclear part of the core-nucleon interaction. Due to the charge symmetry of the strong interaction, these potentials will be the same for both ^{10}Li (^{9}Li $+n$) and ^{10}N (^{9}C $+p$), since also the ^{9}Li and ^{9}C cores are mirror nuclei. Table I contains the parameters used in this work for the potential form given in Eq. (5) with the s- and p-state parameters from Ref. [23]. The

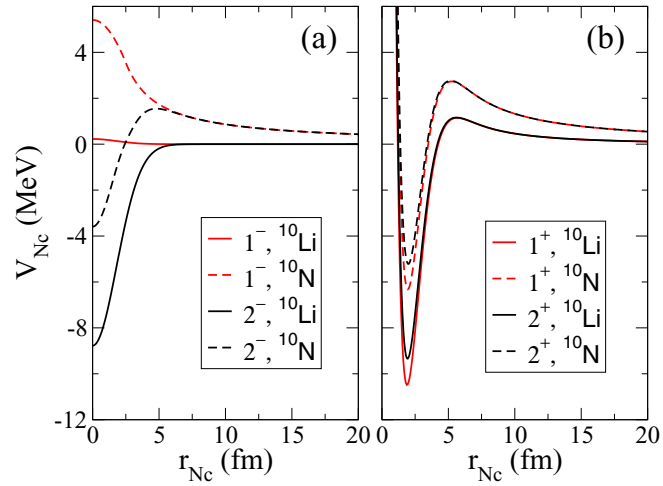

FIG. 1. (a) Core-nucleon potentials for $s_{1/2}$ states, 1^- (red, gray in grayscale) and 2^- (black), in ^{10}Li (solid lines) and ^{10}N (dashed lines). (b) The same as in panel (a), but for the $p_{1/2}$ states, 1^+ (red, gray in grayscale) and 2^+ (black).

radial shapes are for convenience chosen to be Gaussians with the same range in all terms. The actual shape is unimportant as long as it is of short range with a range consistent with the core size.

The two all-decisive properties of the nucleon-core system are the positions of the two-body resonances and the exclusion of Pauli forbidden states occupied by the core nucleons. The first property is achieved by the numerical values specified in Table I. The second property is fulfilled by use of the shallow s-wave potential without a bound state and a large and inverse (positive) sign of the p-wave spin-orbit strength, which places the $p_{3/2}$ shell at an unreachable high energy. In this way, by construction, the valence nucleon can not occupy the Pauli forbidden $s_{1/2}$ and $p_{3/2}$ shells, which already are occupied by the six neutrons or the six protons in the ^{9}Li or ^{9}C core.

The resulting nucleon-core potentials are shown in Fig. 1 for the $s_{1/2}$ states, 1^- (red, gray in grayscale) and 2^- (black) in Fig. 1(a), and for the $p_{1/2}$ states, 1^+ (red, gray in grayscale) and 2^+ (black) in Fig. 1(b). The solid and dashed lines refer, respectively, to the ^{10}Li and ^{10}N cases. The difference between them arises from the Coulomb repulsion entering in the ^{9}C proton interaction for ^{10}N. The s waves in the left panel of Fig. 1 reveal our choices for ^{10}Li of an attractive 2^- potential placing a virtual nucleon-core state very close to zero energy, while in contrast the 1^- potential is very small and slightly repulsive. The same potentials for ^{10}N are pushed up by the Coulomb repulsion, where the 2^- potential still has an attractive short-range part, whereas the 1^- potential is clearly overall repulsive. The p-wave potentials in the right panel of Fig. 1 all have an attractive short-range part leading to more or less known p-wave resonances in both ^{10}Li and ^{10}N.

As shown in Refs. [13,15], the main properties of ^{11}Li, as well as the behavior of the momentum distributions, are essentially determined by the energy of the centroid of the spin-splitted s and p doublets. Therefore, the subsequent three-body results would remain basically unchanged with the

TABLE II. For ^{10}Li, the second column shows the energies of the 1^- and 2^- virtual states and energies and widths of the 1^+, 2^+, and 4^- resonances in ^{10}Li obtained with the two-body potentials described in the text. The third column shows the energies and widths obtained in Ref. [12]. In the fourth column the available experimental data are given [38]. The last column gives the resonance energies computed as $\delta(E_R) = \pi/2$. All the energies, E_R, and widths, Γ_R, are given in MeV.

	This work		Ref. [12]		Expt. [38]		$\delta(E_R) = \frac{\pi}{2}$
	E_R	Γ_R	E_R	Γ_R	E_R	Γ_R	E_R
1^-	–	–	–	–	–	–	–
2^-	−0.020	–	−0.028	–	–	–	–
1^+	0.32	0.19	0.42	0.19	0.42 ± 0.05	0.15 ± 0.07	0.37
2^+	0.58	0.49	0.71	0.40	0.80 ± 0.08	0.30 ± 0.10	0.78
4^-	3.95	2.45	4.13	3.12	4.47 ± 0.10	0.7 ± 0.2	4.88

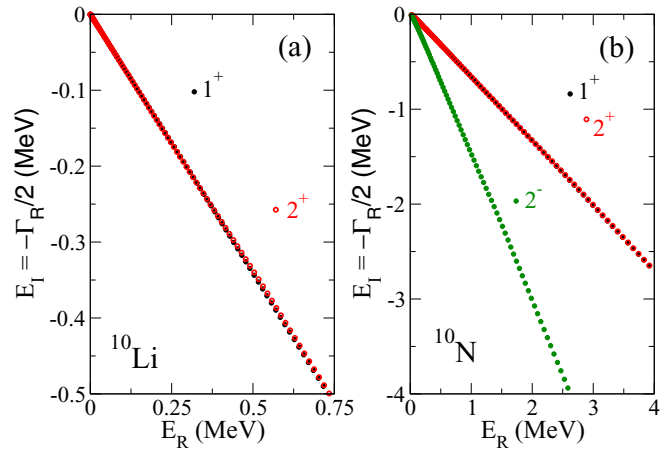

FIG. 2. Complex energies of the $p_{1/2}$ resonances in ^{10}Li (a) and the $s_{1/2}$ and $p_{1/2}$ resonances in ^{10}N (b) after a two-body complex scaling calculation using the potential described in Sec. III.

opposite order of the 1^- and 2^- virtual states and of the 1^+ and 2^+ resonances.

A. ^{10}Li properties

The ^{10}Li properties are determined by the potentials given by the solid curves in Figs. 1(a) and 1(b). The computed spectrum is shown in the second column in Table II. The ground state is a virtual 2^- state resulting from the coupling of an $s_{1/2}$ valence neutron with the $3/2^-$ ground state of the core, whose energy is about −20 keV. The corresponding potential is given by the solid black curve in Fig. 1(a). Due to the repulsive character of the potential shown by the solid red curve in the same figure, the 1^- s-wave partner appears at high energy in the continuum. The p-wave resonant states 1^+ and 2^+, produced by the p-wave potential barriers [solid curves in Fig. 1(b)], are found at 0.32 and 0.58 MeV, respectively, with corresponding widths of 0.19 and 0.49 MeV.

The virtual state is obtained by finding the energy providing the correct divergent asymptotic behavior produced by the poles of the S matrix located on the negative imaginary axis in the complex momentum plane. The resonances are also obtained as poles of the S matrix by means of the complex scaling method [34,35], which simplifies the numerical calculation by giving rise to an exponential fall-off of the complex rotated resonance wave functions. As mentioned in Sec. II, the complex rotated two-body problem is solved after discretization of the continuum by means of a box boundary condition.

The corresponding discrete energies appear in the complex energy plane rotated by an angle equal to twice the angle used for the complex scaling coordinate transformation. The resonances appear as discrete points, independent of the complex scaling angle, and they are located out of the cut (lines) corresponding to continuum states. This is shown for ^{10}Li in Fig. 2(a). As we can see, a complex scaling angle of $\theta = 0.3$ rads is enough to capture the 1^+ and 2^+ resonances. As shown in Table II, together with the 1^+ and 2^+ states, the core-neutron potential described in Sec. III gives rise to a 4^- resonance (with the valence neutron in the $d_{5/2}$ state) at 3.95 MeV with a width of 2.45 MeV. For the sake of clarity in the figure, this resonance is not shown in Fig. 2(a).

The computed spectrum can be compared to the one obtained in Ref. [12] (third column of Table II), where a microscopic coupled-channels calculation is performed. The similar virtual s states in the two calculations are dictated by a demand to reproduce measured two-neutron halo properties of ^{11}Li in subsequent calculations. In the fourth column of the table we give the available experimental data. Note that the ones of the 4^- state are actually in Ref. [38] assigned preliminary to angular momentum and parity, 2^-. However, as suggested in Ref. [12], the calculations might indicate that they could actually correspond to the 4^- resonance.

Although in both this work and Ref. [12] the energies are computed as poles of the S matrix, the agreement with the experimental 1^+ and 2^+ energies [38] seems to be worse in our calculation. The p states deviate somewhat by more than about 100 keV in centroid energy of the two spin-split p states (0.5 MeV in this work and 0.6 MeV in Ref. [12]). However, in Ref. [12] the calculation is performed by fitting the energy of the 1^+S-matrix pole to the experimental energy of the 1^+ resonance, whereas in our case the experimental energies are better reproduced by the energies for which the corresponding phase shifts are equal to $\pi/2$. As seen in the last column in Table II, when computed in this way, our potential gives rise to 1^+ and 2^+ energies equal to 0.37 and 0.78 MeV, respectively, as well as to a 4^- energy of 4.88 MeV.

The differences between resonance energies obtained through the different mathematical definition reflect an intrinsic uncertainty, which only can be resolved by comparing calculations of directly measured observables like specific scattering cross sections. In this connection, it is important that the ^{9}Li neutron interaction used in the present work also leads to reproduction of the experimental excitation energy spectrum of ^{10}Li after the breakup reaction, $d(^9\text{Li}, p)\,^{10}$Li, initiated by a ^{9}Li laboratory energy of 11.1 MeV/nucleon, see Ref. [23].

TABLE III. For ^{10}N, energies and widths, in MeV, of the 1^-, 2^-, 1^+, and 2^+ resonances obtained in our calculation (second column), the theoretical values given in Ref. [25] (third column), and the experimental values given in Refs. [20,21] (fourth and fifth columns). The last column gives the resonance energies computed as $\delta(E_R) = \pi/2$. (*) Although in Ref. [20] the observed resonance was assigned to be an s-wave resonance, as indicated in Ref. [26], it is very likely the energy and width corresponding to the 1^+ state.

	This work		Ref. [25]		Ref. [20]*		Ref. [21]		$\delta(E_R) = \frac{\pi}{2}$
	E_R	Γ_R	E_R	Γ_R	E_R	Γ_R	E_R	Γ_R	E_R
1^-	–	–	–	–	–	–	$1.9^{+0.2}_{-0.2}$	$2.5^{+2.0}_{-1.5}$	–
2^-	1.74	3.94	1.51	3.47	–	–	$2.2^{+0.2}_{-0.2}$	$3.1^{+0.9}_{-0.7}$	–
1^+	2.62	1.68	2.84	1.89	$2.6^{+0.4}_{-0.4}$	$2.3^{+1.6}_{-1.6}$	–	–	3.51
2^+	2.89	2.21	3.36	2.82	–	–	–	–	4.45

B. ^{10}N properties

The mirror nucleus, ^{10}N, is now assumed to have exactly the same potentials as ^{10}Li, except for the Coulomb interaction arising from the substituted valence proton. We assume pointlike protons and a spherical and homogeneously charged ^{9}C core. With these interactions we now compute the spectrum of ^{10}N as described by a ^{9}C core and a proton. The immediate consequence of the Coulomb repulsion is that all the core-nucleon potentials are pushed up in energy, reducing the depth of the potentials and increasing the potential barriers. This is precisely as seen by comparing the dashed and solid curves in Fig. 1.

For the $s_{1/2}$ states the Coulomb barrier implies that the 1^- and 2^- states in principle might appear as resonances. However, the overall repulsive behavior of the 1^- potential (dashed red curve, gray in grayscale, in Fig. 1) does not exhibit any barrier, and only 2^- resonant states are then possible. As for ^{10}Li, resonances in ^{10}N are obtained after a complex scaling calculation. The results are shown in Fig. 2(b), where the resonances are the isolated points located out of the cut (line) associated with the continuum states. The ground state, the s-wave 2^- state, is clearly broader than the 1^+ and 2^+ p states and therefore requires a larger angle in the complex scaling transformation in order to be captured in the calculation. In particular, the calculation shown in the figure has been made using a complex scaling angle equal to 0.5 rads for the 2^- state and 0.3 rads for the 1^+ and 2^+ states.

The resonance energies and widths obtained for ^{10}N are collected in the second column of Table III, where the results are compared to the values given in Refs. [20,21,25]. Our results are very consistent with the theoretical values given in Ref. [25], where the complex scaling method also is used. The slightly different energies are due to a core-nucleon strong interaction producing also slightly different energies for the ^{10}Li states, see Table II. The experimental value in Ref. [20] was initially assigned to a 1^- state, but in Ref. [26] it is suggested that this resonance is very likely the mirror of the probable 1^+ state at 0.24 MeV in ^{10}Li.

Finally, in Ref. [21] (fifth column in Table III) two resonances have been measured with energies around 2.0 MeV, which are assigned by the authors to states with angular momentum and parity, 1^- and 2^-. In this reference the authors mention as well an excited 1^- or 2^- resonant state with an energy of 2.8 ± 0.2 MeV. As seen in Fig. 2(b), we have not found any trace of such an excited state with negative parity. It is in any case striking that the three energies reported in Ref. [21] agree reasonably well with the three energies obtained in this work for the 2^-, 1^+, and 2^+ states.

Due to its large resonance width, the 2^- phase shift never reaches the value of $\pi/2$, and therefore the energy of this resonance cannot be extracted in this way. In contrast, this is possible for the 1^+ and 2^+ states, and this happens for energies equal to 3.51 and 4.45 MeV, respectively, which is clearly larger than the energies obtained as poles of the S matrix (last column in Table III). Again these different definitions reflect in themselves an inherent uncertainty in the resonance parameters.

IV. THE CORE-NUCLEON-NUCLEON SYSTEM

After discussing the two-body properties of ^{10}Li and ^{10}N, we now investigate the effects they determine for the structure and properties of the three-body mirror nuclei ^{11}Li and ^{11}O. We shall do this in three different steps; first, in this section we present the energy spectra, and in the two following sections we discuss the properties of the different states, respectively the internal structure of the wave functions and the spatial distribution of the three constituents.

A. Energy spectrum of ^{11}Li

The potentials used to describe ^{11}Li are the same as used in Ref. [16], where the properties of the computed $3/2^-$ ground-state wave function in ^{11}Li are described. An effective three-body force is used to fit the experimental two-neutron separation energy of 369.15(65) keV [17], which leads to a charge root-mean-square (rms) radius of 3.42 fm, also in agreement with the experimental value reported in Ref. [17]. In this work an attractive Gaussian three-body force with a range of 5 fm and a strength of -0.6 MeV has been used. In addition, as shown in Ref. [16], the computed ^{11}Li ground-state wave function permits reproduction of the experimental energy-integrated angular differential cross section for the ^{11}Li(p, d) ^{10}Li reaction at 5.7 MeV/nucleon.

In Ref. [18] the electric dipole excitations in ^{11}Li, i.e., the $1/2^+$, $3/2^+$, and $5/2^+$ resonant states, were investigated by means of the complex scaling method [34,35]. It was found that the energies of these three resonances are pretty close to each other, with specific values depending slightly on the

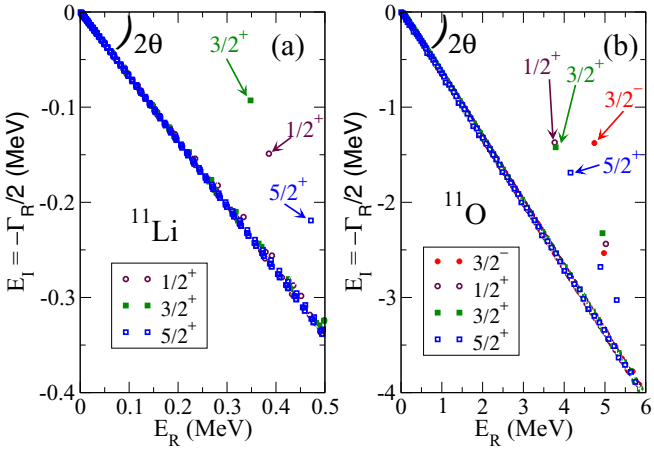

FIG. 3. Complex resonance energies for the computed $1/2^+$ (open brown circles), $3/2^+$ (solid green squares), and $5/2^+$ (open blue squares) states in ^{11}Li (a) and ^{11}O (b), where the $3/2^-$ resonance (solid red circles) is also shown. The calculations have been performed with a complex scaling angle of $\theta = 0.3$ rads.

properties of the core-neutron interaction. In any case, they lie in the energy interval between 0.3 and 0.7 MeV above the three-body threshold.

When the specific interactions used in this work are employed, the complex scaling method reveals the existence of $1/2^+$, $3/2^+$, and $5/2^+$ resonances. The results are shown in Fig. 3(a), where specific dots appear clearly separated from the straight line corresponding to the background continuum states. The resonances of interest are indicated by the arrows in the figure. The precise computed values for the resonance energies and widths, (E_R, Γ_R), are (0.39, 0.30) MeV, (0.35, 0.18) MeV, and (0.47, 0.44) MeV for the $1/2^+$, $3/2^+$, and $5/2^+$ states, respectively. This is also given in the second column in Table IV as a complex number for each state.

B. Energy spectrum of ^{11}O

As expected, due to the Coulomb repulsion, the ground state in ^{11}O is not bound. Therefore, in this case all the states, $J^\pi = 3/2^-$, $1/2^+$, $3/2^+$, and $5/2^+$, will be computed by means of the complex scaling method. We have used a complex scaling angle of $\theta = 0.30$ rads, and the result of the calculation is shown in Fig. 3(b). The straight line, rotated by an angle equal to 2θ, contains the discretized continuum states, and the points out of this line correspond to the different resonances. The lowest $3/2^-$, $1/2^+$, $3/2^+$, and $5/2^+$ states are indicated by the corresponding arrows.

As seen in the figure, in all the cases a second resonance is found in the vicinity of $E_R = 5$ MeV. In the $5/2^+$ case even a third resonance around 5.5 MeV is seen. In order to make the plot clean, the cuts associated to the two-body resonances, i.e., two-body resonance plus the third particle in the continuum [35], are not shown in the figure.

The precise values of the resonant energies, E_R, and widths, Γ_R, are given in the second column of Table V for the two lowest resonances for each of the computed J^π states. As seen in the table, the $1/2^+$, $3/2^+$, and $5/2^+$ energies are similar to each other, especially the $1/2^+$ and $3/2^+$ states, which are almost degenerate. Therefore, very likely one of these states should actually be the ground state, since the $3/2^-$ energy is at least 0.6 MeV higher.

At this point, we emphasize that the computed resonance energies and widths have been obtained without inclusion of any three-body force in the radial Eqs. (4). When a short-range effective three-body potential is included, we have observed that the effect is clearly bigger for the $3/2^-$ state than for the positive-parity resonances. This is an indication that for the $3/2^-$ case the core and the two valence-protons are clearly closer to each other than for the $1/2^+$, $3/2^+$, and $5/2^+$ states.

In particular, if we use a Gaussian three-body force with a range of 5 fm and an attractive strength of -4 MeV, then the energies and widths of the positive-parity resonances remain essentially unchanged, whereas for the lowest $3/2^-$ state we get an energy of 3.72 MeV (with a width of 1.18 MeV), similarly to the one of the other resonances. The conclusion is then that from the pure three-body calculation it is difficult, or even impossible, to determine which J^π state is actually the ground state in ^{11}O. In any case, it seems clear that we cannot exclude the possibility that another state than the $3/2^-$ state becomes the ground state in ^{11}O.

In Table V we compare our results with previous works. In all of them, the ground state is assigned to an angular momentum and parity, $3/2^-$. Only in Refs. [19,22] is the

TABLE IV. Computed complex energies, $E_R - i\Gamma_R/2$, of the $\frac{3}{2}^-$, $\frac{1}{2}^+$, $\frac{3}{2}^+$, and $\frac{5}{2}^+$ states in ^{11}Li, the Coulomb shift for each of them as defined in Eq. (6), and the estimated complex energies of the corresponding states in ^{11}O. All the values are given in MeV.

	^{11}Li (Comp.)	$\Delta_c^{(1)}$	^{11}O (Estim.)
$\frac{3}{2}^-$	−0.37	4.93	4.56
$\frac{1}{2}^+$	0.39−i0.15	2.69−i0.77	3.08−i0.92
$\frac{3}{2}^+$	0.35−i0.09	3.41−i0.86	3.76−i0.95
$\frac{5}{2}^+$	0.47−i0.22	3.89−i1.20	4.36−i1.42

TABLE V. For ^{11}O, the second column gives the computed energies, E_R, and widths, Γ_R, of the $3/2^-$, $1/2^+$, $3/2^+$, and $5/2^+$ states. The last three columns show the results given in Refs. [19,22], Ref. [27], and Ref. [24], respectively. Both energies and widths are given in MeV.

	This work		Ref. [19,22]		Ref. [27]		Ref. [24]	
	E_R	Γ_R	E_R	Γ_R	E_R	Γ_R	E_R	Γ_R
$\frac{3}{2}^-$	4.74	2.75	4.16	1.30	3.21 ± 0.84	–	4.75	2.51
	4.97	5.07	4.85	1.33	–	–	–	–
$\frac{1}{2}^+$	3.77	2.74			–	–	–	–
	5.02	4.87			–	–	–	–
$\frac{3}{2}^+$	3.79	2.84			–	–	–	–
	4.93	4.65			–	–	–	–
$\frac{5}{2}^+$	4.16	3.38	4.65	1.06	–	–	–	–
	4.89	5.36	6.28	1.96	–	–	–	–

positive-parity state $5/2^+$ also considered. In Refs. [19,22], the computed resonances are clearly narrower than the ones obtained in the present work, and the fact that the two energies given for the lowest $3/2^-$ and $5/2^+$ states are similar to ours, but with the quantum numbers exchanged, is probably just an accidental coincidence. The reason for this difference is difficult to determine. On the one hand, in our work the core is assumed to be spherical in contrast to in Refs. [19,22]. Thus, we have ignored the possibly significant role played by the deformation. On the other hand, in Refs. [19,22] the calculations are performed taking a maximum value for the hypermomentum, $K_{\max}$, equal to 20. As we shall discuss later, this value might be too small to guarantee that convergence has been reached in the calculations.

Our three-body approach treats the constituents as inert particles with central two-body interactions, and it is therefore insensitive to deformation. In any case, as discussed in Ref. [39], for sufficiently weakly bound systems, or in other words, provided the valence nucleons are located at relatively large distance from the core, "the quadrupole deformation of the resulting halo is completely determined by the intrinsic structure of a weakly bound orbital, irrespective of the shape of the core." Furthermore, our phenomenological choice of interaction parameters necessarily accounts for at least part of the effects of the core-deformation.

A further comparison is found in another publication [27], where a clearly lower energy, 3.21 MeV, although with a large error bar, is given for the $3/2^-$ state. However, this energy has not been computed but obtained as an extrapolation using the isobaric multiplet mass equation, whose coefficients are determined after the shell-model computed energies for ^{11}Li, ^{11}Be, and ^{11}B. In addition to these energy properties, it was argued in Ref. [24] that the experimental breakup data given in Ref. [19] can be as well reproduced by only the ground state of ^{11}O, whose energy and width are given in Table V to be 4.75 and 2.51 MeV, respectively, very similar to our lowest $3/2^-$ energy and width.

C. Coulomb shift

Due to the charge symmetry of the strong interaction, the ^{11}O states computed in the previous subsection have been obtained simply by adding the Coulomb potential to the nuclear interactions used to describe ^{11}Li. The repulsive character of the Coulomb interaction, between the two valence protons and between each of the valence protons and the core, is obviously the reason for the increase of the energies.

An estimate of how much these energies should be modified by the Coulomb repulsion can be obtained as the first-order perturbative value of the Coulomb shift:

$$\Delta_c^{(1)} = \langle \Psi(^{11}\mathrm{Li}) | V_{\mathrm{coul}} | \Psi(^{11}\mathrm{Li}) \rangle, \tag{6}$$

where $\Psi(^{11}\mathrm{Li})$ is the three-body ^{11}Li wave function corresponding to a given state but where the valence neutrons are replaced by protons, and the charge of the core is assumed to be the one of the mirror nucleus, ^{9}C. Therefore, $\Psi(^{11}\mathrm{Li})$ in Eq. (6) represents an artificial ^{11}O wave function, which is assumed to have the same structure as the corresponding ^{11}Li state. The V_{coul} potential is the resulting Coulomb interaction between the three pairs of charged particles, where the protons are pointlike and the ^{9}C core is spherical and uniformly charged corresponding to the rms radius of about 2.5 fm. The first-order Coulomb shift, $\Delta_c^{(1)}$, is then the diagonal contribution to the Coulomb shift.

As already mentioned, the $1/2^+$, $3/2^+$, and $5/2^+$ states in ^{11}Li have been obtained by means of the complex scaling method. The wave functions are then complex rotated, and the corresponding value of $\Delta_c^{(1)}$ has to be obtained after complex rotation of the Coulomb potential. In this way $\Delta_c^{(1)}$ will be a complex quantity whose imaginary part can be interpreted as the uncertainty in the energy shift [35]. In other words, the imaginary part of $\Delta_c^{(1)}$ in the $1/2^+$, $3/2^+$, and $5/2^+$ cases permits us to estimate as well the change in the width of the resonance.

In Table IV we give the computed energies of the ^{11}Li states (second column) together with the computed values of $\Delta_c^{(1)}$ for the four states considered (third column). The results depend slightly on how the Coulomb potential is constructed, but the overall size and relations are very well determined. As we can see, the value of $\Delta_c^{(1)}$ is substantially larger for the $3/2^-$ state than for the other three states, which again is an indication of the smaller size of the $3/2^-$ state, since the smaller the system the larger the Coulomb repulsion and therefore the larger the value of $\Delta_c^{(1)}$.

When this shift is added to the ^{11}Li energies, we obtain the estimate for the energies of the ^{11}O states given in the last column of the table. In the case of the $3/2^-$ state, since the ^{11}Li wave function is real, the shift $\Delta_c^{(1)}$ is also real, and an estimate of the width in the $3/2^-$ state in ^{11}O is not possible in this way. As we can see, the estimated energies given in the last column of Table IV are quite reasonable and fairly close to the computed energies given in Table V for the lowest $3/2^-$, $1/2^+$, $3/2^+$, and $5/2^+$ states. The only exception is perhaps the $1/2^+$ state, where a difference of about 0.7 MeV is found.

These similarities show that the variations in the energy shift due to the structure differences, as expected, are relatively small. The difference between the energy shift, $\Delta_c^{(1)}$, for a given state and the experimental energy shift, Δ_c, between the experimental energies is a measure of the structure effect of the Thomas-Ehrman shift, that is, $\Delta_{\mathrm{TE}} = \Delta_c - \Delta_c^{(1)}$. Recent calculations of Δ_{TE} concerning different light mirror nuclei are available in the literature. For example, in Ref. [30] the shift between the mirror system ^{11}Be and ^{11}N was investigated. In Ref. [31] the same was done for ^{12}Be - ^{12}O and ^{16}C - ^{16}Ne, and in Ref. [32] this shift was computed for the case of ^{17}N and ^{17}Ne. In all the cases the value of Δ_{TE} was obtained to be of no more than a few hundreds of keV. These sizes are consistent with the energy difference between the lowest J^π energies obtained in our calculation (Table V) and the estimated energies given in the last column of Table IV.

V. THREE-BODY WAVE FUNCTIONS

The calculation of the ^{11}Li and ^{11}O three-body states has been made including all the components satisfying $\ell_x, \ell_y \leqslant 7$, where ℓ_x and ℓ_y are the relative angular momenta between two of the particles and between their center of mass and the third particle, respectively. The maximum value of the

TABLE VI. Dominant components (larger than 1% probability) in the lowest $3/2^-$, $1/2^+$, $3/2^+$, and $5/2^+$ wave functions in ^{11}Li and ^{11}O in the Jacobi set with the $\boldsymbol{x}$ coordinate defined between the core and one of the valence nucleons. The quantum numbers are as defined below Eq. (3). Note that the core has negative parity.

	Component						%	
J^π	ℓ_x	ℓ_y	L	s_x	S	$K_{\max}$	^{11}Li	^{11}O
$\frac{3}{2}^-$	0	0	0	1	3/2	120	22%	5%
	0	0	0	2	3/2	120	35%	7%
	1	1	0	1	3/2	60	6%	11%
	1	1	0	2	3/2	80	10%	19%
	1	1	1	1	1/2	60	4%	9%
	1	1	1	1	3/2	40	5%	11%
	1	1	1	2	3/2	40	3%	7%
	1	1	1	2	5/2	80	12%	28%
$\frac{1}{2}^+$	0	1	1	1	1/2	121	<1%	5%
	0	1	1	1	3/2	201	30%	37%
	1	0	1	1	1/2	121	6%	6%
	1	0	1	1	3/2	121	7%	6%
	1	0	1	2	3/2	201	42%	41%
	1	2	1	1	3/2	61	7%	5%
	2	1	1	1	3/2	41	1%	<1%
$\frac{3}{2}^+$	0	1	1	1	1/2	101	1%	<1%
	0	1	1	1	3/2	101	1%	1%
	0	1	1	2	3/2	161	9%	7%
	0	1	1	2	5/2	201	34%	32%
	1	0	1	1	1/2	101	1%	1%
	1	0	1	1	3/2	161	8%	7%
	1	0	1	2	3/2	161	5%	4%
	1	0	1	2	5/2	201	36%	43%
	1	2	1	2	5/2	41	2%	4%
$\frac{5}{2}^+$	0	1	1	2	3/2	201	24%	23%
	0	1	1	2	5/2	201	25%	20%
	1	0	1	1	3/2	201	25%	26%
	1	0	1	2	3/2	81	3%	2%
	1	0	1	2	5/2	201	23%	25%
	1	2	1	2	3/2	31	<1%	2%
	1	2	1	2	5/2	31	<1%	2%

hypermomentum, $K_{\max}$, has to be sufficiently large to reach convergence, but for all partial waves it has been taken to be at least 20. In Table VI we give the partial wave decomposition and the components with probability larger than 1% for each of the lowest J^π states. Note here that the use of the complex scaling method permits us to normalize the resonance wave functions as described in Ref. [35]. The quantum numbers in the table are as described below Eq. (3), with the $\boldsymbol{x}$-Jacobi coordinate defined between the core and one of the valence nucleons.

As seen in the table, for these components the $K_{\max}$ value used is pretty large, very likely overdoing the work of getting a well-converged three-body solution, especially for ^{11}Li. A careful analysis of each individual component could certainly reduce the $K_{\max}$ value. As a test, we have performed the same calculations using $K_{\max} = 20$ for all the components. These less-accurate calculations result in an increase of the three-body energies by up to 0.4 MeV for the ^{11}Li states and by up to 1 MeV for the ^{11}O resonances. The only exception is the lowest $3/2^-$ state (bound in the case of ^{11}Li), for which the increase in energy is of about 50 keV for ^{11}Li and of about 200 keV for ^{11}O. This is once more reflecting the smaller size of the lowest $3/2^-$ state compared to the positive-parity states, since the closer the particles are to each other the smaller is the basis necessary to reach convergence.

TABLE VII. The same as Table VI but in the coupling scheme where the core-neutron relative orbital angular momentum ℓ_x couples to the spin of the neutron to provide the angular momentum j_N, which couples to the spin of the core to the total core-neutron angular momentum j_x. The relative orbital angular momentum between the core-neutron center of mass and the second neutron, ℓ_y, couples to the spin of the second neutron to give the angular momentum j_y. Both j_x and j_y couple to the total three-body angular momentum J.

	Component					%	
J^π	ℓ_x	j_N	j_x	ℓ_y	j_y	^{11}Li	^{11}O
$\frac{3}{2}^-$	0	1/2	1	0	1/2	22%	5%
	0	1/2	2	0	1/2	35%	7%
	1	1/2	1	1	1/2	15%	32%
	1	1/2	2	1	1/2	25%	53%
$\frac{1}{2}^+$	0	1/2	1	1	1/2	34%	41%
	1	1/2	1	0	1/2	52%	51%
	1	1/2	2	2	3/2	3%	2%
	1	3/2	0	0	1/2	1%	1%
	1	3/2	1	0	1/2	2%	1%
	1	3/2	1	2	3/2	1%	1%
	1	3/2	2	2	3/2	3%	2%
$\frac{3}{2}^+$	0	1/2	1	1	1/2	2%	2%
	0	1/2	2	1	1/2	45%	39%
	1	1/2	1	0	1/2	51%	52%
	1	1/2	3	2	3/2	<1%	3%
$\frac{5}{2}^+$	0	1/2	2	1	1/2	49%	44%
	1	1/2	1	2	3/2	<1%	1%
	1	1/2	2	0	1/2	49%	52%
	1	1/2	2	2	3/2	<1%	1%

The same decomposition is shown in Table VII but in a coupling scheme more consistent with the mean-field quantum numbers, where the core-nucleon relative orbital angular momentum, ℓ_x, couples to the spin of the nucleon to provide the angular momentum j_N, which in turn couples to the spin of the core to give the total core-nucleon angular momentum, j_x. The relative orbital angular momentum between the core-nucleon center of mass and the second nucleon, ℓ_y, couples to the spin of the second nucleon to give the angular momentum, j_y. Both j_x and j_y couple to the total three-body angular momentum, J.

As we can see, the structure of the $3/2^-$ state changes substantially due to the Coulomb repulsion. In the case of ^{11}Li the $3/2^-$ (bound) ground state contains about 40% of core-neutron p-wave contribution. More precisely, 15% of the wave function corresponds to ^{10}Li in the 1^+ state and 25% to ^{10}Li in the 2^+ state (Table VII). With respect to the s-wave

contribution, even if the 1^- state in ^{10}Li is lying high in the continuum, 22% corresponds to ^{10}Li populating that state.

These characteristics are, however, very different when analyzing the $3/2^-$ state in ^{11}O. The Coulomb repulsion, which pushes up the s-wave core-proton 2^- state by more than 1.5 MeV, turns out to be crucial producing a drastic reduction of the s-wave contribution. In fact, as seen in the upper parts of Tables VI and VII, the p-wave components give 85% of the wave function, whereas the s-wave contribution reduces now from almost 60% in ^{11}Li to only about 12% in ^{11}O.

This result is in contrast to Ref. [22], where the 29% s-wave contribution in the $3/2^-$ state in ^{11}O is even higher than the 25% given for ^{11}Li. This low s-wave content in the ^{11}Li ground-state wave function seems to disagree with previous results in Refs. [14–16], where it is shown that the agreement with experimental momentum distributions and angular differential cross sections requires a p-wave content of about 35–40% in the ^{11}Li ground state or, equivalently, 60–65% s-wave contribution.

For both nuclei ^{11}Li and ^{11}O, the contribution of d waves in the present work is far from substantial, in total of about 3% in both cases, and none of the d-wave components provide more than 1% of the norm. This result seems to contradict the measured increase of about 8.8% [40] of the quadrupole moment in ^{11}Li relative to that of ^{9}Li, which in shell-model calculations in Ref. [41] is explained as due to a significant d-wave contribution of similar size as the one corresponding to p waves.

The small probability of d waves may be related to the lack of deformation of the frozen core as seen by the argument. If the structure of a given deformation is expanded on another, say, body-fixed, deformation, then there must be partial wave components corresponding to this deformation. However, our three-body model provides the full wave function corresponding to that obtained with deformation after, not before, projection of angular momentum and parity. Thus, our model can only say something about the inserted frozen core structure and the calculated valence structure.

However, as discussed in Ref. [40], the measured quadrupole moment could instead be related to an about 10% increase of the charge radius in ^{11}Li compared to the one of ^{9}Li. This increase can be interpreted as due to the neutron halo. The two neutrons in the zero angular momentum ground state produce a distortion of the ^{9}Li core, which effectively corresponds to an increase of the core radius. The initially slightly deformed ^{9}Li core is otherwise in principle maintained in the subsequent three-body calculations without significant effect as argued in Ref. [39]. Using such an increased radius, the neutron-core interaction still must be adjusted to the previously described specific desired properties. These all-decisive phenomenologically obtained interactions guarantee the same resulting three-body structure as obtained with the bare ^{9}Li radius. This is consistent with Ref. [40], where it is stated that there is a striking analogy between the quadrupole moment and the rms charge radius without any additional change of wave function structure.

In any case, a detailed analysis of the quadrupole moment of ^{11}Li requires us to take into account the different sources contributing to the measured value, since the two valence neutrons are mostly on the same side of ^{9}Li: first, the contribution from the original ^{9}Li quadrupole moment; second, the one from the rotation of the ^{9}Li core around the three-body center of mass; and, third and fourth, the one from increased radius and induced deformation of ^{9}Li from the two valence neutrons. From Ref. [1] we know that neutral nucleons polarize the charged core by an amount of the same order as if they were charged. Thus, our model is consistent with all available ^{11}Li data, but for now we leave the complicated quantitative quadrupole moment calculation for future investigations.

Concerning the $1/2^+$, $3/2^+$, and $5/2^+$ resonances, they are all almost completely given by sp interference terms. Only minor contributions from pd interferences are seen, with the largest, as given in the tables, reaching 7% in the $1/2^+$ case. The presence of low-lying p resonances in ^{10}Li and ^{10}N makes the pd interferences more likely than the dp ones, whose weight is always smaller than 1%. In general, we can see that the structure of the three positive-parity resonances does not change significantly by moving from ^{11}Li to ^{11}O. The weight of the different components remains essentially the same in both cases.

An important difference, seen in Table VII, between the structure of the different J^+ resonances, is that only the $1/2^+$ state has substantial contributions from s waves ($\ell_x = 0$) in the nucleon-core 1^- state ($j_x = 1$) in either ^{10}Li or ^{10}N. In contrast, for both the $3/2^+$ and $5/2^+$ resonances only the 2^- s state ($\ell_x = 0$, $j_x = 2$) in ^{10}Li or ^{10}N is substantially populated. In the next section, we shall discuss this difference as responsible for the very different spatial structure of these states. Keep in mind that a similar weight of the different partial-wave components does not necessarily imply a similar spatial distribution of the constituents, which is in fact determined by the radial wave functions $f_n^J(\rho)$ in Eq. (1) and the expansion coefficients $C_q^{(n)}(\rho)$ in Eq. (3). A different ρ dependence can still provide a similar weight of the partial waves after integration of the square of the wave function.

VI. THREE-BODY SPATIAL STRUCTURE

Let us examine now the spatial structure of the ^{11}Li and ^{11}O states. A clean indication of how the core and valence nucleons are distributed in space is reflected by the different two-body rms radii, which in turn permits us to obtain a clear picture of the most probable interparticle distances. We therefore first discuss the radii or second radial moments and afterward the origin in the structures of the wave functions.

A. Radii

Since the complex scaling method has been used in the calculations, the corresponding resonance three-body wave functions are complex rotated. As a consequence, for the resonant states, the rms radii have to be obtained as the expectation value of the square of complex rotated radial distance ($r \to re^{i\theta}$). Therefore, the rms radii are in this case complex quantities, and as described in Ref. [35], the imaginary part is a measure of the uncertainty of the computed value.

TABLE VIII. Computed values, in fm, of $\langle r_{ij}^2\rangle^{1/2}$ and $\langle r_{k,ij}^2\rangle^{1/2}$ for the $3/2^-$, $1/2^+$, $3/2^+$, and $5/2^+$ states in ^{11}Li (upper part) and ^{11}O (lower part), where $\{i, j, k\}$ represent the core (c) and the valence neutrons (n) or the core (c) and the valence protons (p), respectively. The coordinate r_{ij} is the distance between particles i and j, and $r_{k,jk}$ is the distance between particle k and the center of mass of the ij system.

^{11}Li				
J^π	$\langle r_{nn}^2\rangle^{1/2}$	$\langle r_{c,nn}^2\rangle^{1/2}$	$\langle r_{cn}^2\rangle^{1/2}$	$\langle r_{n,cn}^2\rangle^{1/2}$
$\frac{3}{2}^-$	6.4	5.0	5.9	5.7
$\frac{1}{2}^+$	$22.3+i6.3$	$11.7+i3.0$	$16.5+i4.4$	$17.1+i4.9$
$\frac{3}{2}^+$	$13.9+i4.8$	$7.4+i3.4$	$10.4+i4.1$	$10.7+i4.1$
$\frac{5}{2}^+$	$9.4+i4.3$	$3.1+i0.9$	$6.8+i2.0$	$7.0+i2.2$
^{11}O				
J^π	$\langle r_{pp}^2\rangle^{1/2}$	$\langle r_{c,pp}^2\rangle^{1/2}$	$\langle r_{cp}^2\rangle^{1/2}$	$\langle r_{p,cp}^2\rangle^{1/2}$
$\frac{3}{2}^-$	$5.1+i3.9$	$2.8+i2.1$	$3.9+i3.0$	$3.9+i3.0$
$\frac{1}{2}^+$	$12.8+i5.0$	$6.6+i3.0$	$9.3+i4.0$	$9.4+i4.0$
$\frac{3}{2}^+$	$12.2+i5.4$	$6.5+i2.9$	$9.0+i4.1$	$9.0+i4.1$
$\frac{5}{2}^+$	$10.7+i6.2$	$5.2+i3.1$	$7.5+i4.5$	$7.5+i4.6$

In Table VIII we give the rms radii, $\langle r_{ij}^2\rangle^{1/2}$ and $\langle r_{k,ij}^2\rangle^{1/2}$, for the different ^{11}Li (upper part) and ^{11}O (lower part) states. From the right part of the table we notice that for all the states in both ^{11}Li and ^{11}O, the distances $\langle r_{cN}^2\rangle^{1/2}$ and $\langle r_{N,cN}^2\rangle^{1/2}$ are similar to each other, where N can be either neutrons (n) or protons (p). Since the core is about nine times heavier than the nucleon, the value of $\langle r_{N,cN}^2\rangle^{1/2}$ is not far from the distance between the core and the second nucleon, which implies that the two valence nucleons are roughly at the same distance from the core in all the J^π states.

Looking now into the left part of Table VIII, we can see that for the bound $3/2^-$ state in ^{11}Li the neutron-neutron distance is similar to the core-neutron distance, which indicates an equilateral triangular structure with a particle-particle distance of about 6 fm. However, for the resonant states in ^{11}Li and ^{11}O the situation is slightly different, since the nucleon-nucleon distance is roughly 1.4 times larger than the core-nucleon distance. This structure corresponds to an isosceles triangle, where the unequal side (the nucleon-nucleon distance) is about 40% bigger than the two equal sides given by the core-nucleon distance.

It is also interesting to note that the $3/2^-$ state for both nuclei is clearly smaller than the positive-parity resonances. This was already anticipated by the larger effect of the three-body force, the larger value of $\Delta_c^{(1)}$ (Table IV), and the smaller $K_{\max}$ values required to get convergence for the $3/2^-$ states. This is related to the facts that in ^{11}Li the $3/2^-$ state is bound and in ^{11}O the $3/2^-$ wave function has a clearly dominant contribution from two valence protons in a relative p wave with respect to the core (85% according to Table VII). In this structure the potential barrier prevents the protons from moving too far from the core [see the dashed curves in Fig. 1(b)].

On the other hand, as mentioned when discussing Table VII, the $1/2^+$, $3/2^+$, and $5/2^+$ resonances are almost entirely sp structures, which implies that one of the halo nucleons is always populating a core-nucleon s state. As seen in Fig. 1(a), the s-wave potentials do not feel any confining barrier, except the 2^- potential in ^{10}N (dashed black curve), for which the potential barrier is almost a factor of 2 lower than for the p potentials for the same system. As a consequence, the positive-parity resonances are, as seen in Table VIII, significantly bigger than for the $3/2^-$ states.

Also, as already mentioned and shown in Table VII, the contribution of the nucleon-core 1^- state ($\ell_x = 0$, $j_x = 1$) to the J^+ resonances is only substantial for the $1/2^+$ state, whereas for the $3/2^+$ and $5/2^+$ resonances basically all the $\ell_x = 0$ contribution arises through the 2^- state ($j_x = 2$). In the case of ^{11}Li, since ^{10}Li shows a very low-lying 2^- virtual state, the ^{11}Li resonances with a large 2^- component ($3/2^+$ and $5/2^+$) will show a tendency to keep the neutron close to the core, leading therefore to a system smaller than the $1/2^+$ state, where the 1^- components dominates. This is actually seen in the upper part of Table VIII, where the rms radii for the $1/2^+$ state are significantly larger than those of the $3/2^+$ and $5/2^+$ resonances.

In the case of ^{11}O, the 2^- state in ^{10}N is not that low anymore, and it is actually rather broad (see Table III), being then close to disappearing into the continuum. The confining effect of the s-wave 2^- resonance disappears, and the $1/2^+$, $3/2^+$, and $5/2^+$ resonances in ^{11}O have a similar size, see Table VIII.

B. Structure

The origin of the average distance results discussed above can be visualized by means of the structure function

$$F(r_{cN}, r_{N,cN}) = r_{cN}^2 r_{N,cN}^2 \int (\Psi(\boldsymbol{r}_{cN}, \boldsymbol{r}_{N,cN}))^2 d\Omega_{cN} d\Omega_{N,cN}, \tag{7}$$

where N represents either the neutron for ^{11}Li or the proton for ^{11}O, Ψ is the complex rotated three-body wave function of a given J^π state, and Ω_{cN} and $\Omega_{N,cN}$ are the angles defining the directions of $\boldsymbol{r}_{cN}$ and $\boldsymbol{r}_{N,cN}$, respectively. Note that following the normalization criteria described in Ref. [35], the definition of the structure function above is made in terms of the square of the wave function and not in terms of the square of the modulus of the wave function. In principle, the function F depends on the complex scaling angle, but since Ψ is normalized to 1 it is obvious that F satisfies that

$$\int F(r_{cN}, r_{N,cN}) dr_{cN} dr_{N,cN} = 1, \tag{8}$$

which implies that the integral of the imaginary part is equal to zero.

The real part of the structure function F is shown in Figs. 4 and 5 for all the computed states in ^{11}Li and ^{11}O, respectively. For the resonances the complex scaling angle $\theta = 0.3$ rads has been used.

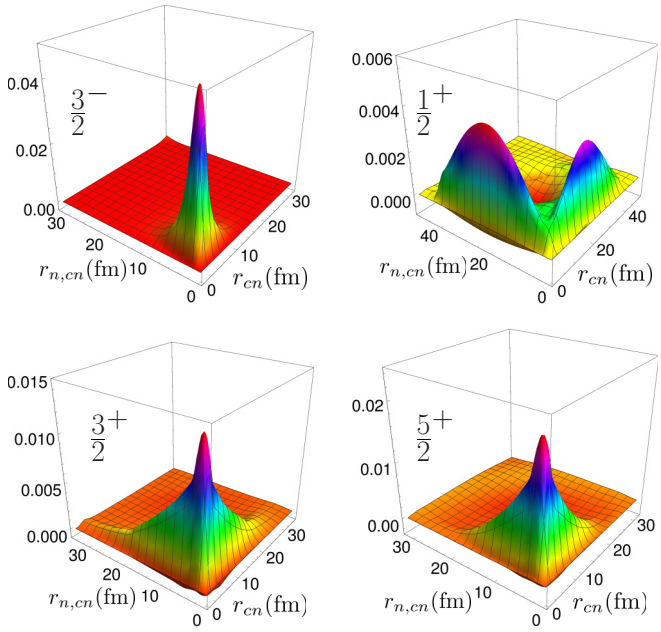

FIG. 4. Real part of the structure function $F(r_{cn}, r_{n,cn})$, as defined in Eq. (7), in fm^{-2}, for the four computed states in ^{11}Li. A complex scaling angle $\theta = 0.30$ rads has been used.

For ^{11}Li, the $3/2^-$ ground-state wave function is rather confined, with a high peak centered around average distances determined by $r_{cn} \approx r_{n,cn} \approx 6$ fm, as expected from the rms radii shown in Table VIII for this state. When looking at the $1/2^+$, $3/2^+$, and $5/2^+$ resonances, we can see that the wave function is progressively developing a tail along the r_{cn} and $r_{n,cn}$ axis, which in turn can be related to the lack of barrier in the s-wave potential. The main difference in the structure function for these three states is the presence of a peak at relatively small core-neutron distances for the $3/2^+$ and $5/2^+$ states. As explained above this is attributed to the important contribution of the 2^- states, which present a very low-lying virtual state. In the $1/2^+$ state this virtual state does not contribute, the peak then disappears, and the wave function shows mainly two wide peaks each located along the two axes.

For ^{11}O, we see in Fig. 5 that the $3/2^-$ resonance shows a structure function with a peak apparently similar to the one of the $3/2^+$ and $5/2^+$ states, although in this case the peak is essentially only of p-wave character. For the $1/2^+$, $3/2^+$, and $5/2^+$ resonances, the s wave contributes significantly, but due the Coulomb repulsion, which pushes up the 2^- resonance in ^{10}N, the s-wave potential is not able to keep the s-wave proton sufficiently close to the core, and the peak observed for the $3/2^+$ and $5/2^+$ states in ^{11}Li disappears.

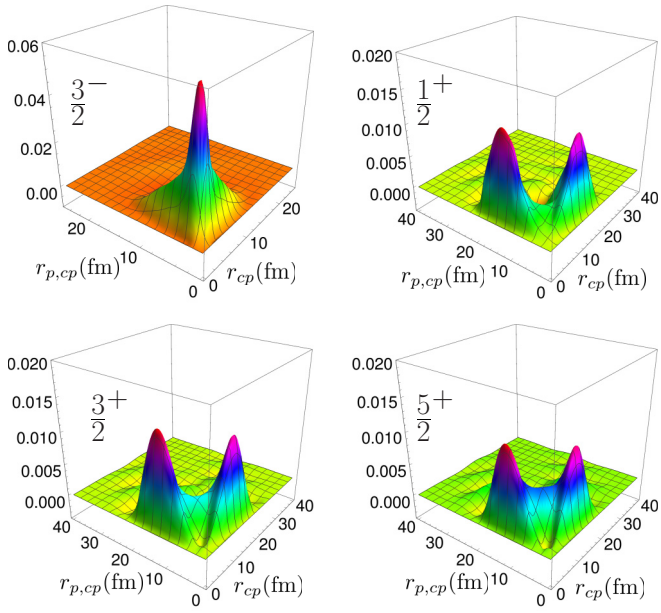

FIG. 5. The same as Fig. 4 for the ^{11}O states.

VII. SUMMARY AND CONCLUSIONS

We have calculated three-body properties of the four lowest excited bound states or resonances for the two light mirror nuclei ^{11}O and ^{11}Li. The phenomenological interactions are chosen to reproduce all known properties of ^{11}Li combined with consistent information about the subsystem, ^{10}Li. The only difference in interactions is that the Coulomb potentials are added in ^{11}O from the charges of the two protons and the ^{9}C core. We use the established hyperspherical adiabatic expansion method combined with complex rotation to separate the resonances from the background continuum structure.

The nuclei ^{11}O and ^{11}Li are special by being nonidentical mirrors on the neutron and proton driplines, that is, at opposite sides of the beta-stability curve. The effect of the Coulomb interactions is rather small for most nuclei, except for a substantial translation of the absolute energies. However, these smaller effects sometimes carry signals about features of interest in a better understanding of many-body nuclear structure. In general the importance lies in change of structure, which requires theoretical models beyond the mean field. A prominent example is the Thomas-Ehrman shift, but in general nuclei at the driplines are expected to maximize such structure variation.

In this report, we predict the properties of ^{11}O and ^{10}N from knowledge of ^{11}Li and its two-body subsystem, ^{10}Li. Other investigations are available, but to our knowledge none consider systematically all four lowest-lying excited states/resonances and their relation to the properties of the nucleon-core subsystems. Furthermore, we use phenomenological interactions, which should enhance the reliability of our predictions. We emphasize that the interactions in the present work are able to reproduce all known features of ^{10}Li and ^{11}Li.

We first investigate the two-body nucleon-core subsystems, proton-^{9}C and neutron-^{9}Li. In realistic calculations the spin-spin splitting is essential, that is, coupling of the $3/2^-$ core and the $1/2^{\pm}$-proton angular momenta and parities. The sequence of the resulting states of 1^- and 2^- is not experimentally determined. Fortunately, the only two crucial properties are, first, the degeneracy weighted centroid energy and,

second, that one of these states is unbound with a marginally negative virtual energy.

The two-body potentials turn out to have attractive pockets at short range for 2^-, while are overall repulsive for the 1^- state. Both receive additional repulsion from the Coulomb potentials in the ^{10}N nucleus. By construction, the 2^- potential for ^{10}Li has a marginally unbound virtual state. Both the 2^+ and 1^+ potentials have attractive short-range pockets for both ^{10}Li and ^{10}N. The resonance energies of course follow the pattern of the potentials with less than 0.6 MeV for all ^{10}Li states and about 2 MeV higher energies for ^{10}N.

The computed three-body energy of ^{11}Li is fine-tuned to reproduce precisely the measured ground-state value, while the three positive-parity excited states of both positions and widths are experimentally unknown but predicted to be very similar. For ^{11}O, we find in contrast to ^{11}Li that the $3/2^-$ state is about 1 MeV higher than the three positive-parity states. The two lowest resonances, $1/2^+$ and $3/2^+$, are very similar, and it is therefore as likely that one of these is the ground state. This would be a qualitative difference between important properties of these mirror nuclei. This predicted energy sequence in ^{11}O is consistent with a perturbation estimate of the Coulomb shift. However, it is important to keep in mind that the uncertainty introduced by the unknown three-body interaction, which is seen to play a more relevant role in the $3/2^-$ state than in the positive-parity states, could modify the ordering in the energy spectrum.

The structure of the wave functions is in principle revealed by the partial wave decomposition. It is striking that the positive-parity resonances all are of very similar partial wave content in ^{11}Li and ^{11}O. In contrast, the $3/2^-$ state in ^{11}O is almost entirely made of p waves of both nucleon-core two-body states, whereas p waves in ^{11}Li only contribute about 40% and s waves correspondingly by 57%.

The spatial distributions of the nucleons surrounding the core also differ substantially in the two nuclei. For the $3/2^-$ state, the two nucleons are symmetrically distributed in one peak in both cases but about 30% closer to the core and more smeared out in the ^{11}O resonance than in the ^{11}Li bound state. The positive-parity resonances in ^{11}O all three exhibit two peaks in their density distributions corresponding to one proton close and one further away from the core. In ^{11}Li, these two peaks coincide for the $3/2^+$ and $5/2^+$ resonances, whereas they remain for $1/2^+$ but with much larger tails. This fact shows that even if the partial wave content is similar (as shown in Table VII for the $3/2^+$ and $5/2^+$ resonances), the spatial distribution of the constituents can be different.

In conclusion, all these detailed predictions are beyond present laboratory tests, but still display essential properties, which in turn should inspire new experimental investigations. The substantial differences between the two mirror nuclei are all due to the additional Coulomb interaction. This is a new experience in nuclear physics, where the Coulomb interaction generally is believed to influence nuclear structure only marginally. In summary, we have learned that mirror nuclei not necessarily have very similar structure. Furthermore, we have seen that dripline nuclei still can deliver new information about nuclear structure.

ACKNOWLEDGMENTS

We thank H. O. U. Fynbo and K. Riisager for drawing attention to these systems and subsequent continuous discussions. We also thank J. Casal for constructive comments and discussions. This work has been partially supported by the Spanish Ministry of Science, Innovation and University MCIU/AEI/FEDER,UE (Spain) under Contract No. PGC2018-093636-B-I00.

[1] A. Bohr and B. R. Mottelson, *Nuclear Structure* (Benjamin, Reading, MA, 1975), Vol II.
[2] V. Zelevinsky and A. Volya, *Physics of Atomic Nuclei* (Wiley-VCH, New York, 2017).
[3] P. J. Siemens and A. S. Jensen, *Elements of Nuclei* (Addison-Wesley, Redwood City, CA, 1987).
[4] W. D. Myers and W. J. Swiatecki, Ann. Phys. **55**, 395 (1969); **84**, 186 (1974).
[5] M. Thoennessen, Rep. Prog. Phys. **67**, 1187 (2004).
[6] M. Freer, Rep. Prog. Phys. **70**, 2149 (2007).
[7] I. Tanihata, H. Hamagaki, O. Hashimoto, Y. Shida, N. Yoshikawa, K. Sugimoto, O. Yamakawa, T. Kobayashi, and N. Takahashi, Phys. Rev. Lett. **55**, 2676 (1985).
[8] I. Tanihata *et al.*, Phys. Lett. B **160**, 380 (1985).
[9] P. G. Hansen and B. Jonson, Europhys. Lett. **4**, 409 (1987).
[10] A. S. Jensen, K. Riisager, D. V. Fedorov, and E. Garrido, Rev. Mod. Phys. **76**, 215 (2004).
[11] L. Johannsen, A. S. Jensen, and P. G. Hansen, Phys. Lett. B **244**, 357 (1990).
[12] K. Kato, T. Yamada, and K. Ikeda, Prog. Theor. Phys. **101**, 119 (1999).
[13] E. Garrido, D. V. Fedorov, and A. S. Jensen, Nucl. Phys. A **700**, 117 (2002).
[14] E. Garrido, D. V. Fedorov, and A. S. Jensen, Phys. Rev. C **53**, 3159 (1996).
[15] E. Garrido, D. V. Fedorov, and A. S. Jensen, Phys. Rev. C **55**, 1327 (1997).
[16] J. Casal, M. Gómez-Ramos, and A. M. Moro, Phys. Lett. B **767**, 307 (2017).
[17] M. Smith *et al.*, Phys. Rev. Lett. **101**, 202501 (2008).
[18] E. Garrido, A. S. Jensen, and D. V. Fedorov, Nucl. Phys. A **708**, 277 (2002).
[19] T. B. Webb, S. M. Wang, K. W. Brown, R. J. Charity, J. M. Elson, J. Barney *et al.*, Phys. Rev. Lett. **122**, 122501 (2019).
[20] A. Lépine-Szily, J. M. Oliveira, Jr., V. R. Vanin, A. N. Ostrowski, R. Lichtenthäler, A. Di Pietro *et al.*, Phys. Rev. C **65**, 054318 (2002).
[21] J. Hooker *et al.*, Phys. Lett. B **769**, 62 (2017).
[22] S. M. Wang, W. Nazarewicz, R. J. Charity, and L. G. Sobotka, Phys. Rev. C **99**, 054302 (2019).
[23] A. M. Moro, J. Casal, and M. Gómez-Ramos, Phys. Lett. B **793**, 13 (2019).

[24] H. T. Fortune *et al.*, Phys. Rev. C **99**, 051302(R) (2019).
[25] S. Aoyama, K. Katz, and K. Ikeda, Phys. Lett. B **414**, 13 (1997).
[26] D. R. Tilley *et al.*, Nucl. Phys. A **745**, 155 (2004).
[27] R. J. Charity, L. G. Sobotka, K. Hagino, D. Bazin, M. A. Famiano, A. Gade *et al.*, Phys. Rev. C **86**, 041307(R) (2012).
[28] J. B. Ehrman, Phys. Rev. **81**, 412 (1951).
[29] R. G. Thomas, Phys. Rev. **88**, 1109 (1952).
[30] N. Auerbach and N. Vinh Mau, Phys. Rev. C **63**, 017301 (2000).
[31] L. V. Grigorenko, I. G. Mukha, I. J. Thompson, and M. V. Zhukov, Phys. Rev. Lett. **88**, 042502 (2002).
[32] E. Garrido, D. V. Fedorov, and A. S. Jensen, Phys. Rev. C **69**, 024002 (2004).
[33] E. Nielsen, D. V. Fedorov, A.-S. Jensen, and E. Garrido, Phys. Rep. **347**, 373 (2001).
[34] Y. K. Ho, Phys. Rep. **99**, 1 (1983).
[35] N. Moiseyev, Phys. Rep. **302**, 212 (1998).
[36] D. Gogny, P. Pires, and R. De Tourreil, Phys. Lett. B **32**, 591 (1970).
[37] E. Garrido, D. V. Fedorov, and A. S. Jensen, Phys. Rev. C **68**, 014002 (2003).
[38] H. G. Bohlen *et al.*, Z. Phys. A **344**, 381 (1993).
[39] T. Misu, W. Nazarewicz, and S. Åberg, Nucl. Phys. A **614**, 44 (1997).
[40] R. Neugart *et al.*, Phys. Rev. Lett. **101**, 132502 (2008).
[41] T. Suzuki, R. Fujimoto, and T. Otsuka, Phys. Rev. C **67**, 044302 (2003).